Int. J. Electrochem. Sci., 17 **(2022)** Article Number: 221117, doi: 10.20964/2022.11.35

International Journal of
ELECTROCHEMICAL
SCIENCE
www.electrochemsci.org

Effect of silicon/carbon composite on properties of Graphite anode materials in Li-ion batteries

Wei Xu[1,2,3], *Chengyuan Ni*[1,*], *Chengdong Xia*[1,**], *Zhongyu Piao*[2], *Wenping Liu*[4]

[1] College of Mechanical Engineering, Quzhou University, Quzhou 324000, China
[2] College of Mechanical Engineering, Zhejiang University of Technology, Hangzhou 310014, China
[3] Key Laboratory of Air-Driven Equipment Technology of Zhejiang Province, Quzhou University, Quzhou 324000, China
[4] Guilin Key Laboratory of Microelectronic Electrode Materials and Biological Nanomaterials & National Special Mineral Materials Engineering Technology Research Center & Guangxi Key Laboratory of Superhard Materials, China Monferrous Metal (Guilin) Geology and Mining Co., Ltd, Guilin 541004，China
*E-mail: nichengyuan1@126.com
**E-mail: xcd309@163.com

Received: 23 July 2022 / *Accepted:* 12 September 2022 / *Published:* 10 October 2022

A carbon coated silicon and carbon coated graphite composites ((Si/C)@C) was prepared from silicon nanospheres, citric acid and graphite. Afterwards, (Si/C)@C was added as an additive to graphite to prepare anode material. The structure, morphology and electrochemical properties of the materials were characterized by XRD, SEM, TEM, and constant current charge/discharge tests. The results showed that the anode material consisted of silicon nanoparticles, graphite and carbon, and the silicon particles coated by an amorphous carbon layer. For graphite with different tap density and morphologies, the addition of (Si/C)@C additives can all improve the electrochemical properties of graphite. Among them, the anode material prepared by adding (Si/C)@C to graphite with high tap density and spherical structure has the best electrochemical performance with an initial discharge capacity of 460 mAh/g, a first coulombic efficiency of 89.8%, and a capacity retention of 87% after the 500th cycle.

Keywords: Lithium ion battery, plasma nanosilicon, spray drying method, silicon carbon composite anode material

1. INTRODUCTION

With the development of various high-end electronic devices and new energy sources, the demand for lithium-ion batteries in various fields is gradually increasing, and the traditional graphite anode materials gradually fail to meet the new requirements, such as cycle life, energy density, volume

change, safety, etc. Therefore, new material lithium-ion batteries with high energy density and long cycle life are needed [1-3]. For lithium-ion batteries, high energy density means that the electrode material can provide a larger capacity per unit volume, and longer cycle life means a more stable anode active material and solid-liquid interface structure, and these characteristics can be improved by developing anode materials [4]. As the most important component of lithium-ion batteries, the specific capacity of anode materials plays a crucial role in increasing the energy density of batteries and largely influences the capacity and performance of lithium-ion batteries. Among them, silicon anode materials have high theoretical specific capacity (4200 mAh/g) and abundant storage capacity, and have the advantages of low discharge/charge voltage and high cost performance. However, silicon materials also have some disadvantages, with silicon swelling up to 300% during lithiation, which often leads to unstable SEI (solid electrolyte interface) films and active material shedding, affecting cell stability, resulting in low cycle life and low cycle efficiency [5-7]. In addition, pure silicon has poor electrical conductivity, low first-time coulombic efficiency, and ineffective capacity release under high current conditions.

To improve the cycling stability of lithium-ion batteries, common approaches include the use of silicon nanoparticles and silicon-carbon composites to reduce the effect of silicon swelling by moderate nanosizing of silicon and preparation of structurally stable silicon-carbon composites [4, 8]. Silicon-carbon composites have several different structures such as carbon-loaded silicon structures [9], carbon-coated silicon structures [10-12], porous structures [13-15], and core-shell structures [16-18]. Among them, carbon-coated silicon is a commonly used silicon-carbon composite structure to improve the electrochemical properties of the material. Jana [10] rapidly froze a homogeneous mixture of silicon nanofibers and superconducting carbon black in a furfuryl alcohol solution and then converted the furfuryl alcohol to carbon to make a carbon coating uniformly covering the nanofibers. This method improves the conductivity of the electrode and provides flexibility to manage the volume expansion during lithiation and desulfurization. It achieved a Coulomb efficiency of 99.6% and a reversible specific capacity of up to 778 mAh/g after 200 cycles. Cui [19] injected Si nanoparticles inside a bilayer of carbon nanotubes to form a sandwich-like structure. The prepared materials exhibited excellent electrochemical properties and cycling stability with high capacity retention. The specific capacity is still as high as 1310 mAh/g after 100 cycles at 100 mA/g and 1050 mAh/g after 500 cycles at 100 mA/g, with a Coulomb efficiency of 98%. It can be seen that the carbon-coated silicon structure does improve the capacity and stability of the material. However, the directly prepared carbon-clad silicon material requires more charge/discharge cycles to bring the Coulomb efficiency above 99.5%.

In this paper, a silicon-carbon composite graphite-based anode material was prepared by incorporating (Si/C)@C composite into graphite. The (Si/C)@C composite material was prepared by spray drying pyrolysis method using silicon nanospheres, citric acid and graphite as raw materials, which has high energy density but low first coulombic efficiency and cannot meet the usage requirements. Therefore, the material was added to graphite as an additive to prepare anode materials with high initial discharge capacity and first coulombic efficiency.

2. EXPERIMENTAL PROCEDURES

2.1 Preparation of the materials

Nanosilicon was prepared from commercial crystalline silicon using a radio frequency induction plasma system with reference to the preparation method of Liu et al [20]. The synthesis process of the anode material is shown in Fig. 1. The anode material was prepared by spray drying and stirring, followed by mixing the (Si/C)@C composite with graphite. The specific experimental procedure is as follows: First, 6 g (6%) of citric acid was dissolved in 100 ml of ethanol, 10 g of silicon nanoparticles were added, ultrasonically dispersed, and stirred for 30 min to form a mixed solution. Then, 4.0 ml of CMC (sodium carboxymethyl cellulose, 4%) was added to 4.0 ml of deionized water in a 500 ml beaker, followed by 80 g (80%) of graphite (Graphite I), and stirred at high speed for 20-30 min. The mixed solution prepared in the first step was added to the dispersed graphite mixture in the second step, stirred uniformly for 10 min (20 wt% solids, to be washed with 100 ml of water) and started spraying. The spraying process was carried out by adjusting the inlet temperature to 200°C and the spray drying pump rate to 800 ml/h. Finally, nitrogen protection and sintering were carried out, with a ramp-up rate of 3 °C/min and maintaining a temperature of 400 °C for 3 h, followed by a ramp-up to 800 °C and a temperature maintenance of 4 h. The (Si/C)@C composites can be obtained by natural cooling.

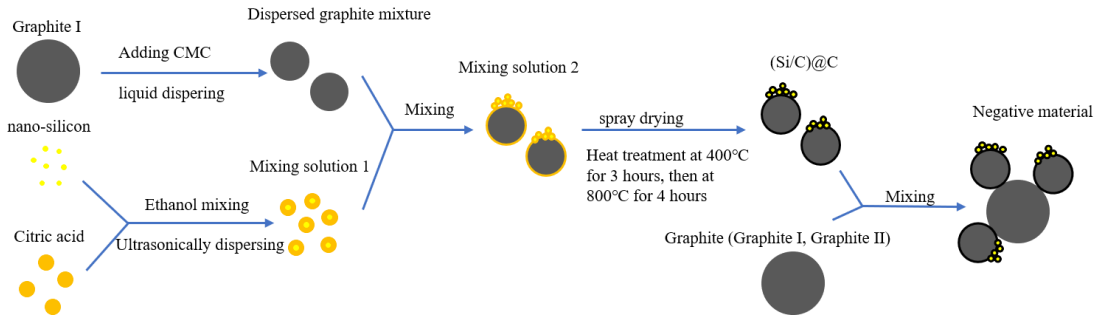

Figure 1. Schematic procedure for the fabrication of Negative material

To better investigate the electrochemical properties, the composites were mixed with graphite(Graphite I, Graphite II), graphite I and graphite II are obtained by purchase. The (Si/C)@C composite and the artificial graphite powder I were mixed in the ratio of 1:4 and recorded as sample 1. The (Si/C)@C composite and the artificial graphite powder II were mixed in the same ratio and recorded as sample 2. The graphite powder I had an irregular volume distribution with a smaller average particle diameter than the graphite powder II. Graphite powder II has a lamellar structure.

2.2 Material characterization

The phases of the prepared samples were examined with an X' Pert PRO X-ray diffractometer (XRD, scan range: 20° to 100°, scan rate: 8°/min, scan power: 15KV 300mA). 8°/min, scan power: 15KV 300mA), and the experimental data were analyzed by Jade. The surface and cross-sectional

morphology of the prepared samples were observed with a Qunta 200 electron microscope (SEM) from the Netherlands, and the visual structure of the internal structure of the particles was examined with a JOEL JSM-2100F transmission electron microscope (TEM). The carbon content in the carbon-silicon composites was detected by Raman spectroscopy.

2.3 Electrochemical characterization

The 80 wt% (Si/C)@C composite, sample 1 and sample 2 were used as active materials, 10 wt% acetylene carbon black (Super P) as conductive agent and 10 wt% carboxymethyl cellulose sodium salt (CMC: Aladdin LR) as binder, respectively. The above three substances were added to the container in the mass ratio of 80:10:10 in turn, and deionized water was added and stirred for 4 hours to prepare a paste, and the resulting mixture was uniformly applied to the copper foil at 80°C. The electrode sheet was obtained by drying under vacuum for 10 hours.

A CR2032 type button cell was prepared using a lithium metal plate as the positive electrode, a prepared electrode sheet as the negative electrode, a Celgard 2300 as the separator, and 1 mol/L $LiPF_6$ as the electrolyte. The battery was placed in a blue LAND BT charge/discharge tester for charge/discharge testing. The test temperature was 30°C the test current density was 0.20 mA/g, the voltage range was 0.01-1.5V, and the scan rate was 0.1 mV/s-2.0 mV/s.

3. RESULTS AND DISCUSSION

3.1 Materials characterization

The SEM images of graphite I and graphite II are shown in Fig. 2a and b, respectively (graphite powder was tested by Fangda Carbon New Materials Co., Ltd. and the actual measurement report of lithium battery anode material is shown in Table 1). As can be seen in Fig. 2a, graphite I has an irregular volume distribution with micrometer diameter and nanometer thickness, and particle size distribution between 16 and 18.5 μm, with an average measured particle diameter of 17.46 μm by BT-9300S Baxter laser particle size test. Fig. 2b shows the SEM image of graphite II. It has a laminar structure with multiple particles stacked together and a particle size distribution between 7 and 11 microns, with an average diameter of 8.46 microns. Fig. 2c shows the SEM image of the (Si/C)@C composite, which shows that the (Si/C)@C composite consists of nearly spherical nanoscale particles with uniform particle size and good dispersion. Moreover, the (Si/C)@C composite is based on graphite, and the silicon particles are uniformly distributed on the surface of graphite particles through an amorphous carbon layer, and the surfaces of both silicon and graphite particles are covered by the amorphous carbon layer. The amorphous carbon layer on the surface of both silicon and graphite particles not only avoids direct contact between the electrode material and the electrolyte, but also reduces the specific surface area of the composite, thus greatly reducing the irreversible capacity of the composite.

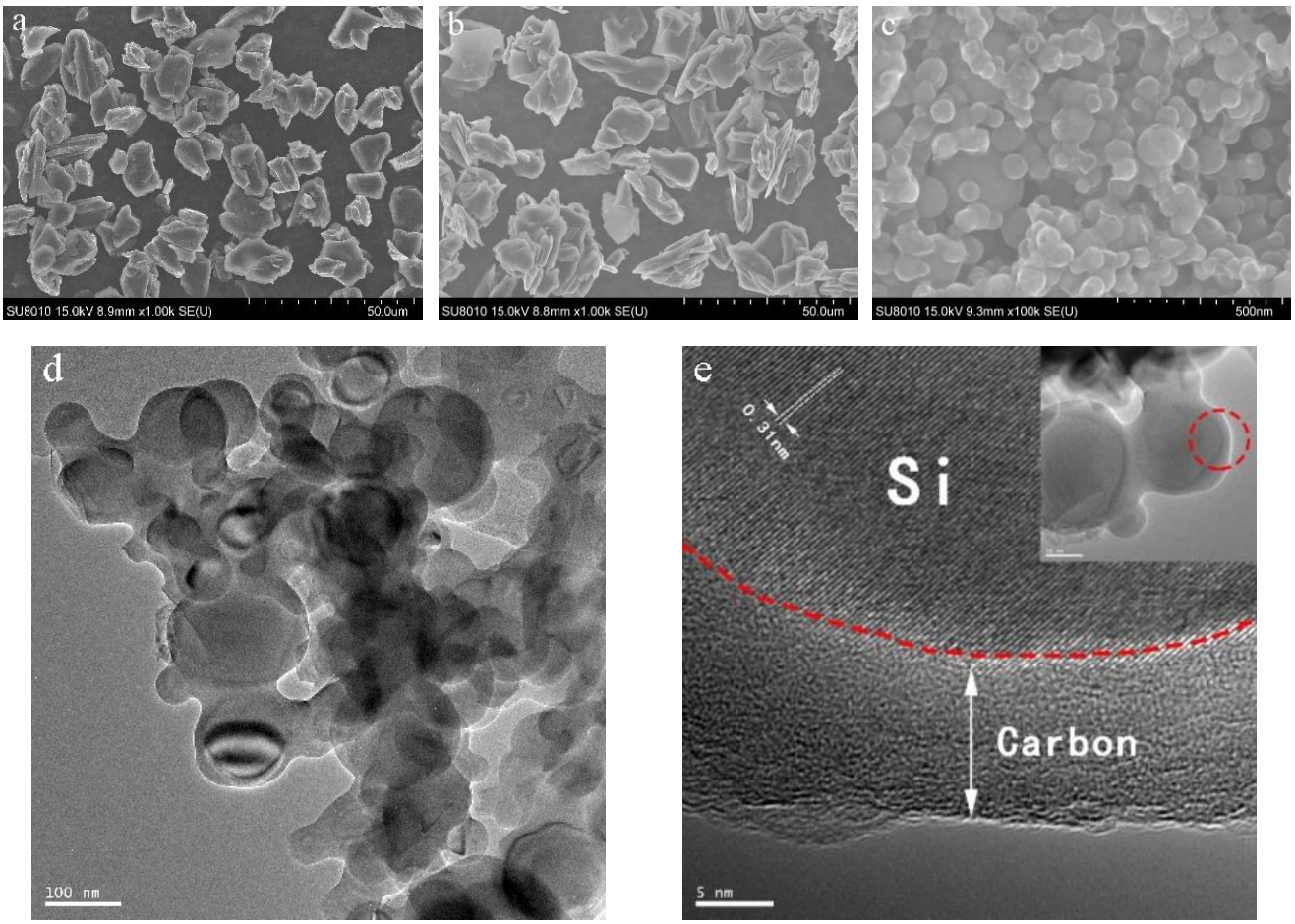

Figure 2. SEM image of graphite I(a), graphite II(b) and (Si/C)@C composite(c), TEM image of a directly prepared (Si/C)@C composite(d-e)

Fig. 2d-e shows the TEM images of the directly prepared (Si/C)@C composites. From the images, it can be seen that there is a clear flocculated carbon coating and silicon nanomaterials, and the silicon nanoparticles are uniformly wrapped by carbon, where the silicon nanomaterials are striped with a spacing of about 0.31 nm between adjacent planes, corresponding to the (111) crystallographic plane of Si, and the thickness of the carbon coating is about 10 nm. the clear spacing of the stripes between planes indicates the relatively high crystallinity of the carbon-silicon composite, a feature that is observed in transmission electron microscopy and scanning electron microscopy is observed differently. Furthermore, in the region of Fig. 2d, in addition to the carbon-coated silicon, some silicon particles without carbon attachment were found exposed on the surface, further indicating that the amorphous layer of a few nanometers thin present on the surface is amorphous carbon.

The graphite interlayer distance is 0.335 nm, and the theoretical specific capacity reaches 370 mAh/g [21]. The smaller layer spacing of graphite material makes the diffusion rate of lithium ions low and the multiplicative performance poor [22]. The addition of silicon nanoparticles encapsulated by an amorphous carbon layer to graphite improves the electrochemical properties of graphite. The layer spacing of amorphous carbon material is larger than that of graphite, which improves the diffusion rate of lithium ions and thus the high current charge/discharge performance of graphite material. The

theoretical specific capacity of silicon nanoparticles is larger than that of graphite, which improves the specific capacity of the material.

Table 1. lithium battery anode material test report

Material Category / Measured Values Items	Artificial Graphite（I）	Artificial Graphite（II）
Particles size (μm)（D50）	17.46	8.46
Tap Density（g/cm^3）	0.762	0.37
Specific Surface Area（m^2/g）	7.242	22.242
Capacity Rate（mAh/g）	345.6	342.8
Initial Efficiency（%）	90.27	87.27

Fig. 3 shows the XRD patterns of pure silicon, sample 1 and sample 2. As can be seen in the figure, sample 1 and sample 2 contain less silicon and the XRD patterns show diffraction peaks of silicon at 2θ=28.5°, 47.3°, 56.1° and 69. 1° corresponding to (111), (220), (311) and (400) crystal planes, respectively, and diffraction peaks of carbon at 2θ=26.4°, 42.2°, 44.4° and 54.5° corresponding to ((002), (100), (101) and (004) crystal planes, respectively. The dispersion peaks in the images are not broadened, which is related to the fact that the composite pyrolytic carbon is an amorphous carbon structure, and only diffraction peaks of crystalline silicon and graphitic carbon are present in the samples, and no peaks of SiO_2 or SiC impurities are evident in the XRD patterns [23]. According to the analysis of the Jade software, the presence of face-centered cubic silicon phase and hexagonal tightly packed structural carbon phase in the sample. In summary, it is indicated that the prepared anode materials (sample 1, sample 2) are mainly composed of silicon, graphite and carbon materials, and the (Si/C)@C additive and graphite did not react chemically during the processing and were physically mixed to produce a new phase.

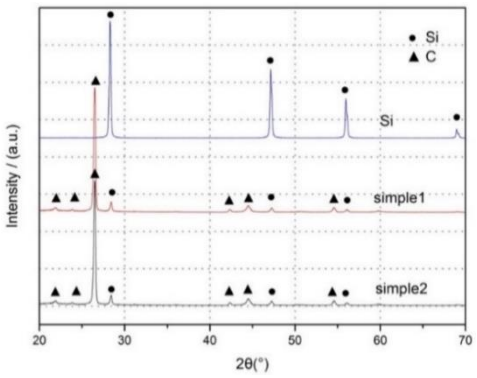

Figure 3. The XRD patterns(a) of Pure silicon, sample 1, sample 2

Fig. 4 shows the Raman spectrum of the (Si/C)@C composite. As seen in the Fig. 4, Raman spectrum exhibits a silicon intensity peak at a wavelength of 502 cm^{-1} and the other two peaks are in the D and G bands at wavelengths of 1311 cm^{-1} and 1583 cm^{-1}, respectively. The D band describes the (Si/C)@C composites with amorphous carbon, while the G band corresponds to graphite [24-25]. Also, the low ratio of D-band intensity to G-band (about 0.83) indicates that the graphite structure in (Si/C)@C composites has good order and fewer defects, which ensures the electrical conductivity and strength of the composites.

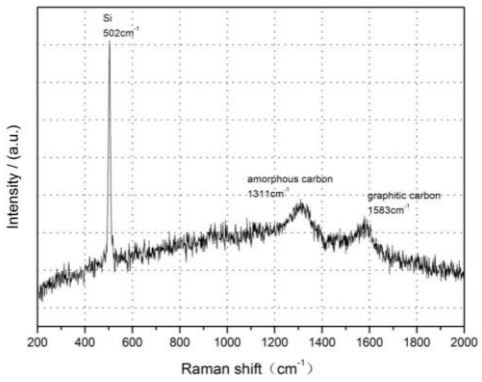

Figure 4. Raman spectrum(b) of (Si/C)@C composite

Fig. 5 shows the SEM images of the (Si/C)@C composite electrode, sample 1 electrode. As shown in Fig. 5a-b, the SEM images of the directly prepared electrodes are similar, and the initial structures of the two electrodes are similar. However, as shown in Fig. 5c-d, more lithium dendrites appeared on the (Si/C)@C composite electrode after 500 cycles, and significantly fewer lithium dendrites were found in the electrode of sample 1, indicating that the electrochemical cycling characteristics of sample 1 were more stable. The possible reason is that sample 1 has more graphite content and its structure is more stable, which reduces the generation of lithium dendrites.

The irregular deposits formed by the reduction of lithium ions during the charging process of lithium batteries are called lithium dendrites. During charging and discharging, a layer of SEI (solid electrolyte interface) film is generated at the interface between electrode material and electrolyte, on the one hand, the formation of SEI (solid electrolyte interface) film will consume some lithium ions and reduce the battery capacity, on the other hand, the SEI (solid electrolyte interface) film is insoluble in organic solvents, which can avoid the damage caused by solvent molecules to the electrode material [26,27]. Therefore, maintaining the stability of the SEI (solid electrolyte interface) film is beneficial to improve the battery cycling stability. sample 1 and (Si/C)@C composite consist of silicon nanoparticles, graphite and carbon, with more graphite in sample 1. The excessive volume expansion of silicon during lithium ion embedding and de-embedding can damage the SEI (solid electrolyte interface) film, and the poor electrical conductivity can make the lithium ion de-embedding process more irreversible and promote lithium dendrite generation. Graphite has strong electrical conductivity and elasticity, so the increase of graphite content improves the electrical conductivity of the material and reduces the generation of lithium dendrites, thus reducing the destruction of the SEI (solid electrolyte interface) film.

Moreover, the increase of graphite content reduces the damage of SEI (solid electrolyte interface) film due to the expansion of silicon, thus improving the stability of the material.

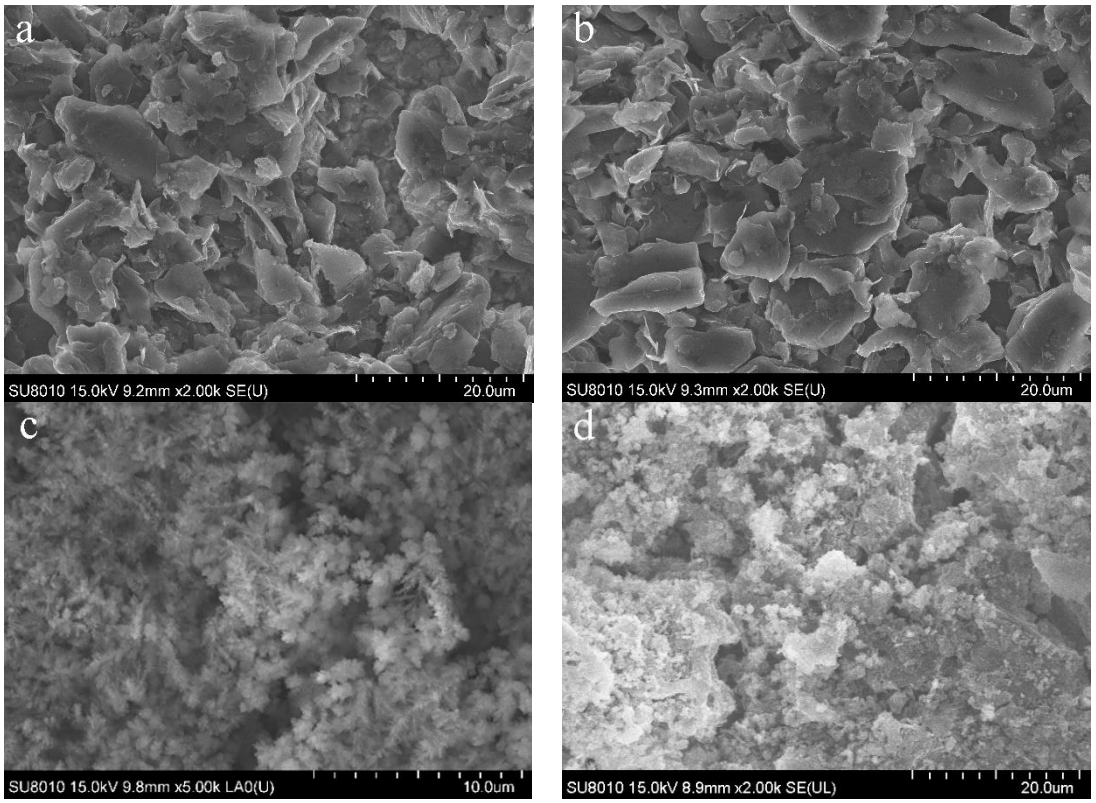

Figure 5. SEM images of (a) (Si/C)@C and (b) sample 1 electrodes before cycling with $LiPF_6$ as electrolyte, (c) (Si/C)@C and (d) sample 1 electrodes after 500 cycles with $LiPF_6$ as electrolyte

3.2 Electrochemical properties

The electrochemical properties of the (Si/C)@C composites were tested as shown in Figure 6. As can be seen from Fig. 6, the initial discharge specific capacity of the (Si/C)@C composite is 750 mAh/g with a first coulombic efficiency of 92.3%, and after 500 cycles, the discharge specific capacity of the (Si/C)@C composite is 415.5 mAh/g with a capacity retention rate of 55.4%. Compared with pure silicon materials, (Si/C)@C composites encapsulate an amorphous carbon layer on the surface of silicon particles, and amorphous carbon has a higher reversible specific capacity to buffer the volume change and prevent the destruction of the SEI(solid electrolyte interface) film [28,29].

However, since the capacity retention of the (Si/C)@C composites could not meet the requirements for use, the prepared (Si/C)@C composites were added to different graphite powders for charge/discharge cycling tests. Fig. 6 shows the cycling performance and cycling efficiency images of (Si/C)@C composites, sample 1 and sample 2. It can be seen from the figure that the initial discharge specific capacities of (Si/C)@C composite, sample 1 and sample 2 were 750 mAh/g, 460 mAh/g and 450 mAh/g, respectively, with first coulombic efficiencies of 92.3%, 89.8% and 91.9%. After the 500th cycle, the discharge specific capacities of (Si/C)@C composites, sample 1 and sample 2 reached 415.5 mAh/g, 400 mAh/g and 377 mAh/g. At this time, the capacity retention rates were 55.4%, 87.0% and

83.8%, respectively. Meanwhile, the cycling efficiencies all reached more than 99% after 500 cycles of the process. In summary, the (Si/C)@C composite has a reversible capacity of 450 mAh/g, but the cycle life and stability are poor, and when it is mixed with graphite, a composite with higher capacity than graphite and good stability and cycle life can be obtained. Fig. 6b shows the Coulomb efficiency of the (Si/C)@C composite, sample 1 and sample 2 in the first 40 cycles. Among them, sample 1 has the best cycling stability with more than 99.5% coulombic efficiency in less than 20 cycles. Sample 1 had the same type of graphite and a higher content compared to the (Si/C)@C composite.

The cycling performance and efficiency results of the three samples indicate that the use of carbon-coated silicon structures to prepare the materials facilitates the formation of a stable SEI(solid electrolyte interface) layer on the silicon anode surface, which can improve the coulombic efficiency and reversible specific capacity of the materials. The addition of (Si/C)@C composites into graphite can improve the cycle life, coulombic efficiency and cycle stability of (Si/C)@C composites.

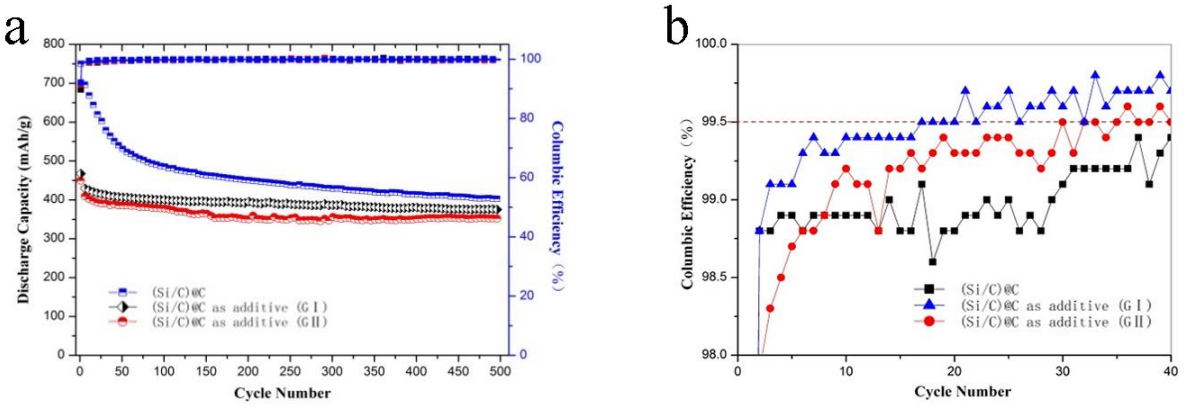

Figure 6. Cycle performance (a) and cycle efficiency diagram(a)(b) for (Si/C)@C and sample 1 and sample 2 at a temperature of 30°C, current density of 0.20mA/g, voltage range of 0.01-1.5V, and scan rate of 0.1mV/s-2.0mV/s using LiPF6 as electrolyte

To further investigate the effect of (Si/C)@C composites on graphite anode materials for lithium-ion batteries, sample 1 was compared with other graphite-based lithium-ion battery anode materials described in the literature. The current modification methods of graphite-based anode materials for lithium-ion batteries are mainly spheroidization treatment, surface treatment and doping modification, spheroidization treatment and surface treatment improve graphite-based anode materials in terms of first charge/discharge efficiency and cycling stability greatly, but increase the specific capacity little, while doping treatment combines the advantages and disadvantages of the incorporated materials and can significantly increase the specific capacity, but will reduce the cycling stability and first coulombic efficiency[30]. Sample 1 was prepared by directly mixing the artificial graphite with the (Si/C)@C composite, which increased the initial discharge capacity of sample 1 and decreased its first coulombic efficiency. As shown in Table 2, the final obtained sample 1 has an initial discharge capacity of 460 mAh/g and a first coulomb efficiency of 89.8%, comparing with other graphite-based anode materials,

sample 1 has good electrochemical properties including high initial discharge capacity and first coulomb efficiency.

Table 2. Modification strategies and electrochemical properties of graphite-based anode materials for lithium batteries reported in the literature

Modification strategy	Electrochemical performance (capacity, an initial columbic efficiency)	Reference
Silicon nanoparticles and bitumen-coated carbon shells coated on graphite surface (surface treatment)	400 mAh/g, 83.04%	[17]
Phenolic resin thermally cracked carbon cladding on phosphor flake graphite surface (surface treatment)	360 mAh/g, 89.7%	[31]
Natural phosphor flake graphite as negative electrode material	360 mAh/g, 92%	[32]
Preparation of Si/C composites by high energy ball milling and pyrolysis (doping modification)	690.6 mAh/g, 70.57%	[33]
Bonding and drying of ultrafine graphite powder into isotropic regular spherical particles (spheronization treatment)	372 mAh/g, 80%	[34]
Direct mixing of artificial graphite with (Si/C)@C composites	460 mAh/g, 89.8%	Sample 1

In order to investigate the reason why (Si/C)@C composites can improve the electrochemical properties of graphite. Since the electrochemical properties of sample 1 are better than sample 2, and the reasons for the improved electrochemical properties of samples 1 and 2 are similar the (Si/C)@C composites and sample 1 were prepared as simulated cells and tested separately. After repeated charge/discharge performance tests, the charge/discharge curves were obtained as shown in Fig. 7a-b. It can be clearly seen that the charge/discharge curves of (Si/C)@C composite and sample 1 are similar. Fig. 7a shows the charge/discharge curves of the (Si/C)@C composite. The (Si/C)@C composite starts with a sloping slope on the initial discharge curve at 0.6-0.8 V, which corresponds to the formation of the SEI(solid electrolyte interface) film and the decomposition process of the electrolyte. The plateau at 0-0.1 V corresponds to the embedding process of lithium in the crystalline silicon, and as the number of cycles increases, the SEI(solid electrolyte interface) film continues to form and the lithium ions continue to be embedded in the silicon and cannot be reversibly removed, resulting in irreversible capacity increase and a decrease in charge/discharge specific capacity [35,36].

The charge/discharge curves of the (Si/C)@C composite in Fig. 7a showed a rapid decay in capacity, so the (Si/C)@C composite was added to graphite. Several charge/discharge performance tests were conducted on the obtained composite anode material, and the images obtained are shown in Fig.

7b. At this point, the capacity decay of the (Si/C)@C composite slowed down with the increase of the number of cycles, and the charge/discharge curves tended to be consistent, indicating that sample 1 has good stability. This is because graphite has strong electrical conductivity and elasticity, which can buffer the volume expansion and improve the electrical conductivity of the material [36].

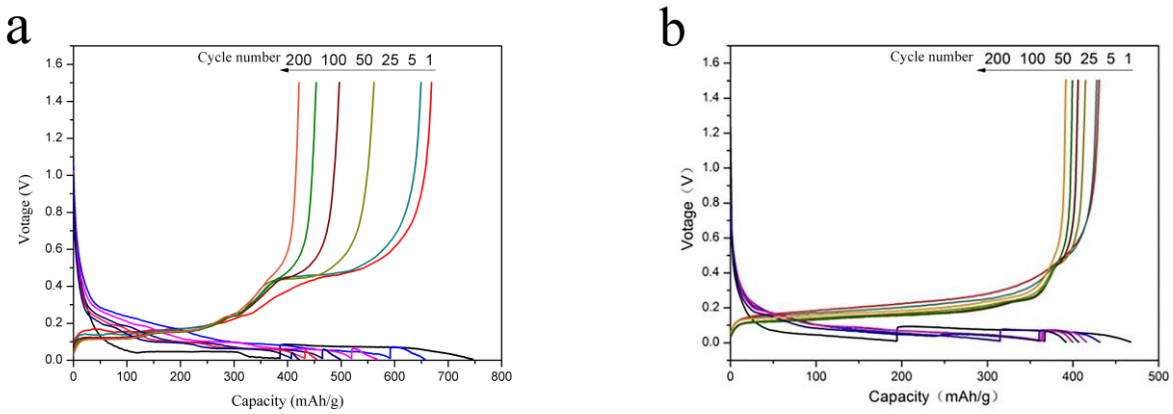

Figure 7. Discharge/charge curves of (a)(Si/C)@C composite, (b)sample 1 at a temperature of 30°C, current density of 0.20mA/g, voltage range of 0.01-1.5V, and scan rate of 0.1mV/s-2.0mV/s using LiPF6 as electrolyte

In order to further investigate the difference of (Si/C)@C composites addition to different graphite, the cyclic voltammetric behavior of samples 1 and 2 was investigated. Fig. 8 shows the cyclic voltammetry curves of samples 1 and 2 in the voltage range of 0.01-1.5 V at scan rates from 0.1 mV/s to 2.0 mV/s. It can be seen from Fig. 8 that the cyclic voltammetry curves of samples 1 and 2 are similar, but at the same time there are some differences in some cyclic voltammetry behaviors. As can be seen from Fig. 8a, at the scan time of the negative electrode, when the scan rate is 0.1 mV/s, a reduction peak appears at 0.75 V, corresponding to the decomposition of electrolyte and the formation of SEI(solid electrolyte interface) film, and the peak drifts about 0.15 V with increasing scan rate, and the current decreases with increasing scan rate. When the anode is scanned, two oxidation peaks appear at 0.25 V and 0.45 V, corresponding to the de-lithiation process in crystalline silicon. As the rate increases, the oxidation peaks move to higher potentials and the current increases with the scan rate. As shown in Fig. 8b, the reduction peak disappears and the oxidation peak moves to a lower potential compared to sample 1 for sample 2. The lithium ion intercalation/desorption process of sample 2 has a lower voltage and less formation of lithium dendrites. This phenomenon facilitates high current charging and discharging to ensure battery safety.

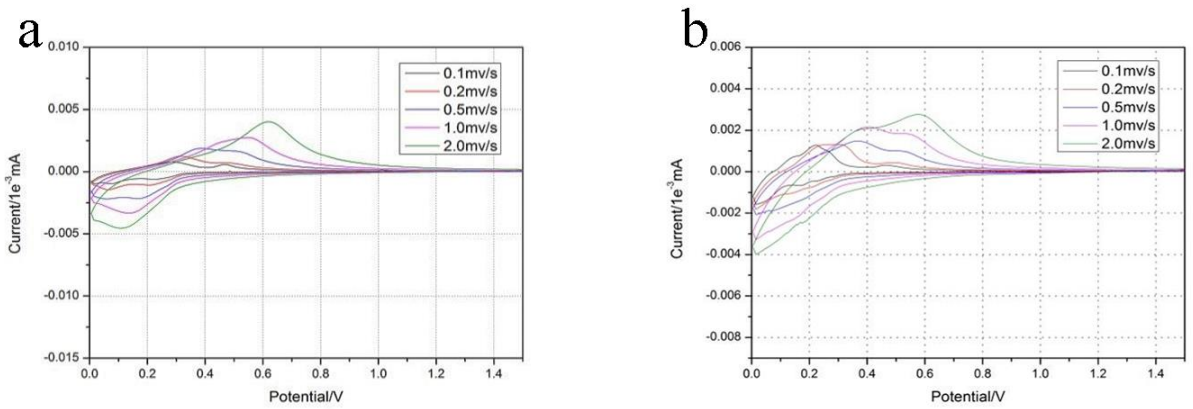

Figure 8. Cyclic voltammetry curves for (a) Sample 1 and (b)Sample 2 at voltages from 0.01 V to 1.5 V and scan rates from 0.1 mV/s to 2.0 mV/s

A linear fit of Ip and $v^{0.5}$ for samples 1 and 2 was performed and the graph obtained is shown in Fig. 9. The diffusion coefficient D can be calculated according to the equation $I_p=2.99 \times 10^5 n（\beta_{n\beta}）^{0.5} S C_0 v^{0.5} D^{0.5}$ [37], where I_p is peak current. n- is electron transfer number. $\beta_{n\beta}$ is transfer coefficient of the active substance. S is effective area of the electrode, cm2. C_0 is concentration of the active substance on the electrode surface, mol/cm^3. v is scanning velocity, mV/s. Dis diffusion coefficient, cm/s. The diffusion coefficient D1 of sample 1 is 3.6×10^{-9} cm/s, while the diffusion coefficient D2 of sample 2 is 0.88×10^{-9} cm/s. The results indicate that the lithium ions in sample 1 have a faster diffusion rate and better high current discharge capability. The reason may be that the shape and tap density of graphite affect the cyclic voltammetric behavior of the material, graphite with high tap density and spherical structure has better rate and cycle performance than graphite with low tap density and lamellar structure [38].

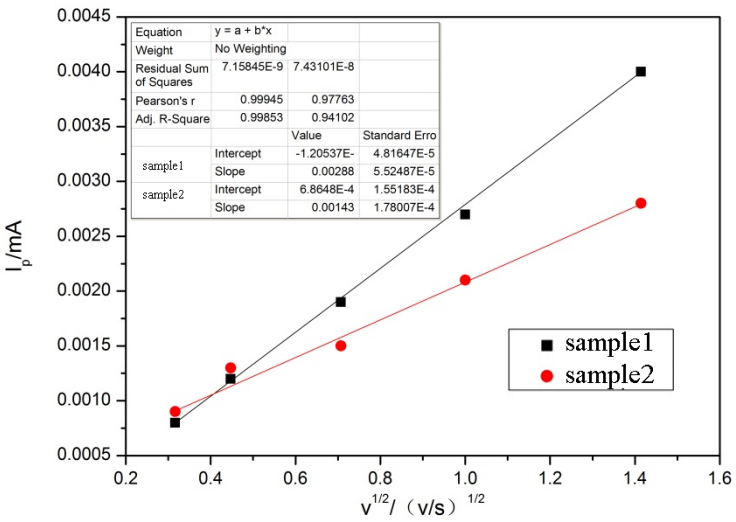

Figure 9. Linear fit curve between I_p and v1/2 of sample 1 and sample 2.

4. CONCLUSIONS

(1) The (Si/C)@C composites exhibit high initial discharge specific capacity, low cycle life and stability. The negative electrode materials (sample 1 and sample 2) mainly consisted of silicon, graphite and carbon, and the silicon particles were coated by an amorphous carbon layer with a thickness of about 10 nm, which prevented the destruction of the SEI(solid electrolyte interface) film and reduced the generation of lithium dendrites.

(2) The incorporation of (Si/C)@C additives into graphite with different particle sizes and different morphologies all improved the electrochemical properties of graphite. The best electrochemical performance was obtained for sample 1, which exhibited high initial discharge specific capacity (460 mAh/g), high first coulombic efficiency (89.8%) and high stability (capacity retention of 87.0% after 500 cycles).

(3) Graphite morphology and tap density affect the cyclic voltammetric behavior of the material. The faster lithium ion diffusion rate in sample 1 is due to the rate and cycling performance of graphite with high tap density and spherical structure than graphite with low tap density and flake structure.

ACKNOWLEDGEMENT
This work was supported by Quzhou Science and Technology Bureau(Grant No.2021K26), the Scientific and Technological Plan of Guilin City (20210207-4) and the Joint Funds of the Zhejiang Provincial Natural Science Foundation of China (Grant No. LZY22E010002).

References

1. S. Chen, F. Dai and M. Cai, *ACS Energy Lett*., 5 (2020) 3140.
2. B. Liu, R. Fang, D. Xie, W. Zhang, H. Huang, Y. Xia, X. Wang, X. Xia and J. Tu, En*ergy Environ. Mater.*, 1 (2018) 196.
3. M. Zheng, H. Tang, L. Li, Q. Hu, L. Zhang, H. Xue and H. Pang, *Adv. Sci.,* 5 (2018) 1700592.
4. Q. Liu, S. Y. Hao, D. Feng, Y. Mei and T. B. Zeng, *Acta Mater. Compos. Sin*., 39 (2022) 1446.
5. S. J. Zhao, Y. Z. Ma, Y. C. Xie,G. S. Song and R. Z. Huang, *Chin. J. Power Sources*, 45 (2021) 673.
6. S. Park, J. Sung, S. Chae, J. Hong, T. Lee, Y. Lee, H. Cha, S. Y. Kim, J. Cho, *ACS. Nano*., 14 (2020) 11548.
7. W. An, B. Gao, S. Mei, B., Xiang, J. Fu, L. Wang, Q. Zhang, P.K. Chu and K. Huo, *Nat. Commun*., 10 (2019) 1447.
8. F. Liu, L. J. Qin and Y. X. Liu, *Mod. Chem. Ind*., 37 (2017) 14.
9. X. Kuang, X. Li, S. Li, J. Xiang and X. Wang, *J. Microelectromech. Syst*., 27 (2018) 201.
10. M. Jana, T. Ning and R. N. Singh, *Mater. Sci. Eng. B-Adv*., 232–235 (2018) 61.
11. Y. Xue and Z. Lin. *Chinese J. Inorg. Chem*., 35 (2019) 537.
12. M. K. Kim, W. H. Shin and H. M. Jeong, *Appl. Surf. Sci*. , 467–468 (2019) 926.
13. Y. Son, N. Kim, T. Lee, Y. Lee, J. Ma, S. Chae, J. Sung, H. Cha, Y. Yoo and J. Cho, *Adv. Mater*., 32 (2020) 2003286.
14. X. Fan, B. Yin, T. Wu, M. Feng, G.C. Zhang, S. Li, S. Tang, J. Gu, B. Wen and L. Lu, *Energy Technol.,* 7 (2019) 1800787.
15. F. Wang, L. Sun, W. Zi, B. Zhao and H. Du, *Chem. Eur. J*., 25 (2019) 9071.
16. Z. Wang, N. Yang, L. Ren, X. Wang and X. Zhang, *Microporous Mesoporous Mater.*, 307 (2020)

110480.
17. A. Yin, L. Yang, Z. Zhuang, Q. Feng, Z. Liu, T. Chen, F. Tu, Q. Peng, L. Luo, G. Tang, W. Chen, S. Qin and J. Wu, *J. Energy Storage*, 2 (2020) e132.
18. K. Wang, S. Pei, Z. He, L. Huang, S. Zhu, J. Guo, H. Shao and J. Wang, *Chem. Eng. J*., 356 (2019) 272.
19. S. Cui, S. Chen and L. Deng, *Ceram. Int*., 46 (2020) 3242.
20. W. Liu, H. Xu, H. Qin, Y. Lv, F. Wang, G. Zhu, F. Lin, L. Wang and C. Ni, *J. Solid State Electrochem.,*23 (2019) 3363.
21. H. Lu, B. N. Liu, G. Chu, J. Y. Zheng, F. Luo, X. P. Qiu, H. Li, F. Liu, S. N. Feng, W. Chen, H. Hong and L. Q. Cheng, *Energy Storage Sci. Technol.,* 5 (2016) 109.
22. M. Nie, D. Chalasani and D. P. Abraham, *Phys. Chem. C,* 117 (2013) 1257.
23. H. Wu, F. M. Xiao, Y. Wang, R. H. Tang and R. F. Zhou, *Chin. J. Power Sources*, 42 (2018) 941.
24. Y. Miroshnikov and D. Zitoun, *J. Nanopart. Res.,* 19 (2017) 372.
25. Y. Ikoma, K. Hayano, K. Edalati, K. Saito, Q. Guo, Z. Horita, T. Aoki and D. J. Smith. *J. Mater. Sci.,* 49 (2014) 6565.
26. K. Xie, W. Wei, K. Yua, W. Lu, M. Guo, Z. Li, Q. Song, X. Liu, J. G. Wang and C. Shen, *ACS Appl. Mater. Interfaces.,* 8 (2016) 26091.
27. X. B. Cheng, R. Zhang, C. Z. Zhao, F. Wei, J. G. Zhang and Q. Zhang, *Adv. Sci.,* 3 (2015) 1500213.
28. H. Wang and H. B. Chew, *ACS Appl. Mater. Interfaces*, 9 (2017) 25662.
29. Y. Zhou, H. Guo, Z. Wang, X. Li, R. Zhou and W. Peng, *J. Alloys Compd.,* 725 (2017) 1304.
30. J. Shi, Q. Liu, H. Y. Zang and X. J. Lv, *New Chem. Mater.,* 47 (2019) 42.
31. Z. Jian, H. Liu, J. Kuang, Y. He and H Xiao, *Procedia Eng.,* 27 (2012) 55.
32. M. Yoshio, H. Wang, K. Fukuda, T. Umeno, T. Abe and Z. Ogumi, *J. Mater. Chem.* 14 (2004) 1754.
33. C. Li, Y. Q. Guo, H. H. Li, C. L. Wang, H. Y. Chang, X. W. Zhang and Y. Zhou, *Carbon Tech.,* 39 (2020) 11.
34. X. Wu, X. Yang, F. Zhang, L. Cai, L. Zhang and Z. Wen, *Ceram. Int.,* 43 (2017) 9458.
35. P. Guan, L. Liu and Y. Gao, *ECS Trans*., 85 (2018) 1041.
36. S. Gantenbein, M. Schönleber, M. Weiss and E. Ivers-Tiffée, *Sustainability,* 11 (2019) 6697.
37. D. A. Aikens, *J. Chem. Educ.*, 60 (1983) A25.
38. L. B. Rong, G. H. Zhong, Z. J. Li and D. Zhu, *Battery Bimon.,* 48 (2018) 113.